



HAL
open science

COMPASS Upgrade: a high-field tokamak for ITER- and DEMO-relevant research

M. Komm, F. Jaulmes, O. Grover, M. Peterka, J. Seidl, M. Imrisek, S.
Saarelma, P. Snyder, M. Sos, J. Caloud, et al.

► **To cite this version:**

M. Komm, F. Jaulmes, O. Grover, M. Peterka, J. Seidl, et al.. COMPASS Upgrade: a high-field tokamak for ITER- and DEMO-relevant research. Nuclear Fusion, 2024, 64 (7), pp.076028. 10.1088/1741-4326/ad4569 . cea-04829019

HAL Id: cea-04829019

<https://cea.hal.science/cea-04829019v1>

Submitted on 10 Dec 2024









HAL is a multi-disciplinary open access archive for the deposit and dissemination of scientific research documents, whether they are published or not. The documents may come from teaching and research institutions in France or abroad, or from public or private research centers.

L'archive ouverte pluridisciplinaire **HAL**, est destinée au dépôt et à la diffusion de documents scientifiques de niveau recherche, publiés ou non, émanant des établissements d'enseignement et de recherche français ou étrangers, des laboratoires publics ou privés.



Distributed under a Creative Commons Attribution 4.0 International License

COMPASS Upgrade: a high-field tokamak for ITER- and DEMO-relevant research

M. Komm^{1,*} , F. Jaulmes¹ , O. Grover¹, M. Peterka¹ , J. Seidl¹ , M. Imrisek¹, S. Saarelma², P. Snyder³ , M. Sos¹, J. Caloud¹, I. Borodkina¹, O. Shyshkin¹, J. Ceardle¹, M. Farnik¹, J. Gerardin¹, L. Kripner¹, R. Dejarnac¹, J. Horacek¹ , S. Lukes¹, J. Havlicek¹, D. Tskhakaya¹ , M. Hron¹ , R. Panek¹, P. Vondracek¹, V. Weinzettl¹ and the COMPASS Upgrade Team^a

¹ Institute of Plasma Physics of the CAS, Za Slovankou 3, 182 00 Prague 8, Czech Republic

² CCFE, Culham Science Centre, Abingdon OX14 3DB, United Kingdom of Great Britain and Northern Ireland

³ Oak Ridge National Laboratory, Oak Ridge, TN 37830, United States of America

E-mail: komm@ipp.cas.cz

Received 12 January 2024, revised 20 March 2024

Accepted for publication 30 April 2024

Published 3 June 2024



CrossMark

Abstract

To achieve their goals, future thermonuclear reactors such as ITER and DEMO are expected to operate plasmas with a high magnetic field, triangularity and confinement. To address the corresponding challenges, the concept of the high-field ($B_T \leq 5$ T), high-current ($I_p \leq 2$ MA) COMPASS Upgrade tokamak was established, and the device is currently being constructed in Prague, Czech Republic. This contribution provides an overview of the priority physics topics for the future physics programme of COMPASS Upgrade, namely: (i) characterisation of alternative confinement modes, (ii) a power exhaust including liquid metals, (iii) operation with a hot first wall and (iv) the influence of plasma shape on pedestal stability and confinement. The main scenarios are presented, as predicted by METIS and FIESTA codes. Pedestal pressure and density are estimated using EPED, multi-machine semi-empirical scaling and a neutral penetration model. Access to detachment is estimated using a detachment qualifier.

Keywords: tokamak, H-mode, liquid metal, scenario development, power exhaust

(Some figures may appear in colour only in the online journal)

^a See Vondracek *et al* 2021 (<https://doi.org/10.1016/j.fusengdes.2021.112490>) for the COMPASS Upgrade Team.

* Author to whom any correspondence should be addressed.



Original Content from this work may be used under the terms of the [Creative Commons Attribution 4.0 licence](https://creativecommons.org/licenses/by/4.0/). Any further distribution of this work must maintain attribution to the author(s) and the title of the work, journal citation and DOI.

1. Introduction

Thermonuclear reactors such as ITER and European DEMO will operate in conditions which have been optimised to achieve high fusion power and $Q \gg 1$. As such, some parameters of their baseline scenarios will lie outside the range explored by currently operated machines.

Apart from the evident case of a major radius R , the plasma triangularity δ is a notable example of such a parameter. ITER is expected to operate with $\delta = (\delta_u + \delta_l)/2 = 0.5$ ($\delta_u = 0.43$ and $\delta_l = 0.58$) [1], which is significantly higher than what is routinely achieved in single-null plasmas in contemporary tokamaks. Triangularity is known to affect the properties of ELMy H-mode [2], in particular, the presence of large edge localised modes (ELMs) [3], pedestal height [4] and the power decay length [5]. Another such important parameter is the toroidal magnetic field B_T —both ITER and European DEMO expect $B_T \sim 5$ T [1, 6], which is twice the typical values operated, e.g. at ASDEX Upgrade (AUG), DIII-D or JET. To achieve a conventional value of $q_{95} \sim 3 - 4$, operating at high B_T also requires operation with a high poloidal magnetic field, $B_p \sim 1$ T. Multi-machine scaling of the scrape-off layer power decay length λ_q [7] indicated that $\lambda_q \sim B_p^{-1.19}$ (being independent of R), leading to predictions of very short $\lambda_q \sim 1$ mm for ITER. Even though gyrokinetic simulations suggest significantly higher values (~ 5 mm) [8], the projected heat flux footprint would result in an intolerable loading of the divertor targets [9] unless dedicated counter-measures are adopted. This is a strong motivation for intensive research in the field of power exhausts, such as the development of real-time systems for divertor heat flux control, which has been demonstrated on AUG [10], TCV [11], Alcator C-Mod [12], COMPASS [13] and elsewhere. However, with the exception of Alcator C-Mod [12], effective heat flux control has not been established in scenarios with very short power decay lengths.

To fill gaps in the parameter space of the contemporary machines, a new device, COMPASS Upgrade, was proposed [14] and is currently under construction at the site of the former COMPASS tokamak at the Institute of Plasma Physics of the Czech Academy of Sciences in Prague. It is a medium-sized ($R = 0.894$ m, $a = 0.275$ m), high-field ($B_T \leq 5$ T), high-current ($I_p \leq 2$ MA) full-metal tokamak. The baseline plasma shape is designed to mimic the ITER plasma shape ($\delta_u = 0.43$, $\delta_l = 0.58$, $\kappa = 1.8$), with the possibility to establish plasmas with a wide range of triangularities ($0.35 < \delta < 0.65$) and even negative triangularity plasmas with a dedicated set of plasma-facing components (PFCs). COMPASS Upgrade will belong to the new generation of high-field tokamaks, together with SPARC [15], Italian DTT [16] and ITER (their comparisons are summarised in table 1). Strong synergy among these machines is expected, especially within the Eurofusion consortium, where COMPASS Upgrade and I-DTT can complement each other in a similar manner to AUG and JET in the past.

For details of the machine design we refer the reader to an engineering overview [17]. Similarly, the progress in diagnostics design has been already reported [18]. The purpose of this work is to present the priority physics topics, which will

be investigated at this facility, to describe the main scenarios of the future machine and a brief literature overview of the respective topics.

2. COMPASS Upgrade tokamak concept

The design of COMPASS Upgrade [17] was, to a large extent, inspired by Alcator C-Mod [19], which is unfortunately no longer in operation. It will achieve a high toroidal magnetic field using copper coils, which will be pre-cooled to cryogenic temperatures, requiring the presence of a cryostat. As such, the maximum discharge flat-top duration will be approximately 3 s for the nominal value of 5 T. The starting temperature of the first wall components T_{wall} will be variable (regulated by the additional in-vessel heating circuits), with hot wall capability in the later phases of commissioning ($T_{\text{wall}} \leq 500$ °C). This will allow one to investigate the effects of the hot wall on the plasma discharges [20, 21] as well as enabling one to develop and test materials and diagnostics compatible with such high temperatures (which are considered for next-step devices [22, 23]).

COMPASS Upgrade is designed to be a completely carbon-free machine, with the PFCs manufactured from either Inconel or tungsten. This is an advantageous situation in comparison to devices which have been originally operated with carbon PFCs and later upgraded to full-metal components (and which typically still exhibit remaining carbon content in the plasma). As such, COMPASS Upgrade will be capable of fully avoiding the deposition of hydrocarbon layers in shadowed regions of the first wall. Note that these layers can otherwise store significant numbers of hydrogen isotopes [24] and could complicate investigations of wall saturation at elevated first wall temperatures.

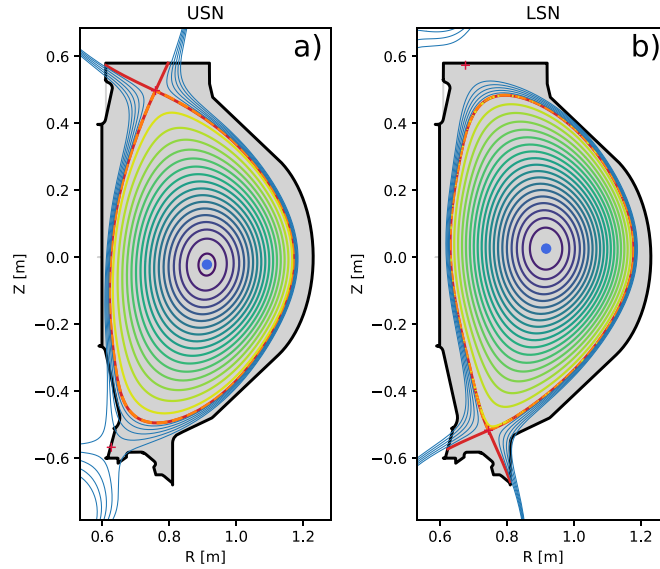
The device will be equipped with a closed lower divertor featuring tungsten PFCs, which will be optimised to handle elevated heat fluxes in high-power scenarios. Later, this divertor will house a full toroidal ring of PFCs based on liquid metal (LM) technology. An initial open divertor with PFCs made of a combination of Inconel and tungsten will be installed on the top, as shown in figure 1. The flexibility of the open divertor geometry will allow one to achieve some of the special regimes, such as the compact radiative divertor (CRD) (see section 4.7).

While the material properties of tungsten for the PFCs have not been specified yet at the time of writing, it will be largely based on the specification of the ITER divertor monoblocks [25]. The shape of the divertor PFCs at the lower outer vertical target was inspired by those at AUG [26], featuring a relatively long poloidal extent (120 mm) but narrow toroidal length (25 mm).

An important difference between COMPASS Upgrade and Alcator C-Mod is the auxiliary heating system. While Alcator C-Mod relied on a combination of lower hybrid and ion cyclotron RF systems, COMPASS Upgrade will be equipped with positive neutral beam injection (NBI) and electron cyclotron resonant heating (ECRH) heating systems. While NBI is

Table 1. A comparison of nominal parameters of currently constructed high-field tokamaks.

| Machine | R/a (m) | B_T (T) | I_P (MA) | P_{in} (MW) | t_{pulse} (s) | Q | First plasma |
|------------|-----------|-----------|------------|---------------|-----------------|-----|--------------|
| COMPASS-U | 0.9/0.28 | 5.0 | 2.0 | 6 | 1–3 | — | 2026 |
| SPARC [15] | 1.9/0.6 | 12.2 | 8.7 | 25 | 10 | 11 | 2026 |
| I-DTT [16] | 2.2/0.7 | 6.0 | 5.5 | 45 | 100 | — | 2029 |
| ITER | 6.2/2.0 | 5.3 | 15 | 75–100 | 1000 | 10 | 2030s |

**Figure 1.** Plasma shapes of the USN early H-mode (a) and LSN ITER-like H-mode (b).

considered as a primary heating system, injecting neutrals with 80 keV energy [27], ECRH (using 140 GHz gyrotrons) will be utilised mainly to maintain high purity of the core plasma. One of the NBI units will be steerable, allowing counter-injection with respect to the standard direction of the plasma current. While these heating methods have clear advantages in terms of coupling of power into the plasma, their performance significantly deteriorates at high densities. The ECRH system has a maximum cutoff density of $2.5 \times 10^{20} \text{ m}^{-3}$ (this density may be lower for specific scenarios, depending on the heating scheme used). In the NBIs, the location of power deposition of 80 keV neutrals is shifting towards the edge plasma for densities above $\sim 3 \times 10^{20} \text{ m}^{-3}$ [28]. Predictions of plasma density and its control are therefore one of the essential points of the focus of the scenario development (see section 5).

3. Main scenarios

COMPASS Upgrade has a mission to be a flexible tool to support ITER and DEMO. This ambition is reflected in the main scenarios, which are considered for its operation (see table 2).

In the first phase of operation, the machine will likely operate with reduced power supplies, limited heating systems (1–3 MW of NBI and 0–1 MW of ECRH) and an incomplete coverage of the PFCs—e.g. without the closed lower divertor. As such, two principle scenarios are envisaged for this phase: *early L-mode* and *early H-mode*. Both are designed to run as

upper single-null (USN) plasmas (see figure 1(A)) at reduced value of $B_T = 2.5 \text{ T}$ and $I_P = 0.8 \text{ MA}$, with strike points on the upper initial open divertor.

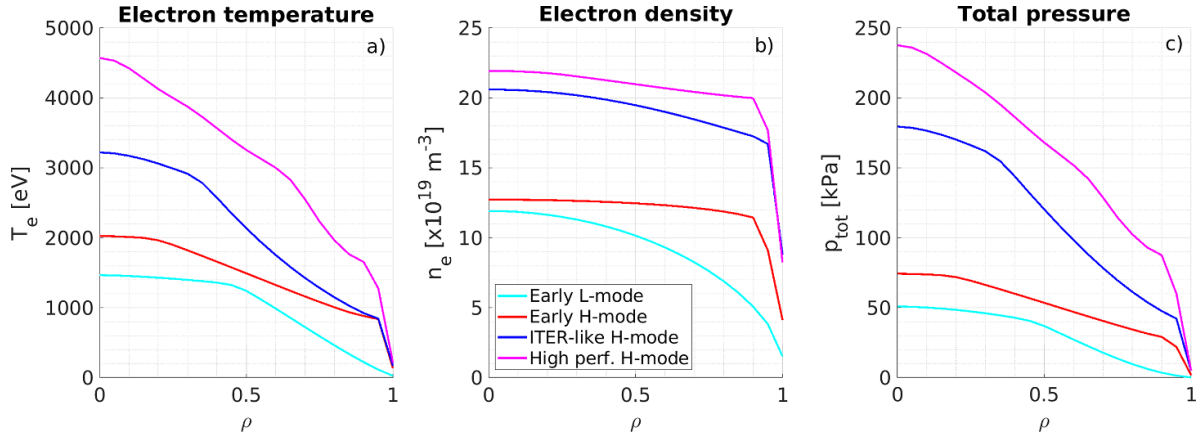
Once the machine reaches the full capacity of the power supply systems, auxiliary heating (4+2 MW of NBI and ECRH) and complete set of the PFCs, the main lower single-null (LSN) scenario, dubbed *ITER-like H-mode* ($B_T = 4.3 \text{ T}$, $I_P = 1.3 \text{ MA}$), will mimic the ITER baseline scenario. In addition, *high-performance H-mode* ($B_T = 5.0 \text{ T}$, $I_P = 1.6 \text{ MA}$) will attempt to achieve the top performance of the machine (e.g. in terms of pedestal pressure). The profiles of temperature, density and pressure for these main scenarios are shown in figure 2. All these scenarios feature a practically identical plasma shape with $\delta_l = 0.58$, $\delta_u = 0.43$, $\kappa = 1.8$ and $R/a = 3.3$. Simulations in METIS [29] and FIESTA [30] were performed to estimate the plasma parameters of these scenarios.

4. Access to modes with improved confinement

High-confinement regimes are expected as baseline scenarios for practically all future thermonuclear reactors. Traditionally, Type I ELMy H-mode was considered the best candidate, serving, e.g. as a baseline scenario for ITER. Recently, alternative high-confinement regimes became the subject of intensive research [31] since they avoid the complications related with the impact of large ELMs while keeping the benefits of high-energy confinement. These alternatives to ELMy

Table 2. The main scenarios for the COMPASS Upgrade physics programme. Auxiliary heating power P_{in} is shown as $P_{NBI} + P_{ECRH}$.

| Name | Scenario | B_T (T) | I_p (MA) | P_{in} (MW) | \bar{n}_e (m^{-3}) | q_{95} | β_n | $T_{e,ped}$ (eV) |
|-------------------|----------|-----------|------------|---------------|--------------------------|----------|-----------|------------------|
| Early L-mode | #3100 | 2.5 | 0.8 | 0+0 | 9.0×10^{19} | 3.2 | 0.67 | — |
| Early H-mode | #3210 | 2.5 | 0.8 | 2+0 | 12×10^{19} | 3.6 | 1.52 | 840 |
| ITER-like H-mode | #24 300 | 4.3 | 1.3 | 3+1 | 19×10^{19} | 3.8 | 1.19 | 820 |
| High perf. H-mode | #5400 | 5.0 | 1.6 | 4+2 | 20×10^{19} | 3.4 | 1.15 | 1360 |

**Figure 2.** Profiles of electron temperature (a), electron density (b) and the total pressure (c) for the main scenarios.

H-mode are mainly (i) enhanced D-alpha (EDA) H-mode [32], (ii) I-mode [33], (iii) quiescent (QH)-mode [34], (iv) quasi-continuous (QCE) mode [35], (v) the X-point radiating regime (XPR) [10], (vi) the compact radiative divertor (CRD) [36] and (vii) negative triangularity [37]. All these modes will be studied at COMPASS Upgrade.

4.1. ELMy H-mode

The access to ELMy H-mode can be characterised by a multi-machine regression by Martin [38] in terms of the minimum required heating power P_{L-H} and its dependence on n_e and B_T

$$P_{L-H}(\text{MW}) = 0.0488 n_e^{0.72} [10^{20} \text{ m}^{-3}] B_T^{0.8} [\text{T}] S^{0.94} [\text{m}^2] \quad (1)$$

where S is the separatrix surface. This scaling, however, characterises only the high-density branch of the dependence. For densities below the optimal value $n_{L-H,\min}$ the P_{L-H} rises sharply with decreasing density [39]. The optimum density was characterised by Ryter [40]:

$$n_{L-H,\min} [10^{20} \text{ m}^{-3}] = 0.07 I_p^{0.34} [\text{MA}] B_T^{0.62} [\text{T}] a^{-0.95} [\text{m}] \times \left(\frac{R}{a} \right)^{0.4}. \quad (2)$$

Numerically, the values of $n_{L-H,\min}$ read 0.6, 1.0 and $1.2 \times 10^{20} \text{ m}^{-3}$ and P_{L-H} read 0.9, 1.9 and 2.5 MW for the early H-mode, ITER-like H-mode and high-performance H-mode scenarios, respectively. As shown in figures 3(A)–(C), the required power is well within the capabilities of the heating

schemes of COMPASS Upgrade by considering the radiated power P_{rad} to be $\sim 30\%$ of the injected power P_{inj} (for early H-mode, even $P_{rad} \sim 0.5 P_{inj}$ should still allow H-mode access).

4.2. EDA H-mode

EDA H-mode is a type of stable, ELM-free H-mode with a good confinement, which makes it a perspective candidate for future thermonuclear reactors. The access to EDA H-mode was thoroughly studied at Alcator C-Mod, where this mode was discovered [41]. Recently, it was also achieved at AUG using ECRH and adequate fuelling [42]. The conditions for power P_{L-EDA} required to access this mode were established in [32] (using Alcator C-Mod data):

$$P_{L-EDA}(\text{MW}) = 0.054 \sqrt{n_{e,L} [10^{20} \text{ m}^{-3}]} B_T^{0.85} [\text{T}] S^{0.84} [\text{m}^2]. \quad (3)$$

This represents the high-density branch of the L-EDA threshold, which was accessible in Alcator C-Mod for densities above $8 \times 10^{19} \text{ m}^{-3}$ (at $B_T = 5.4 \text{ T}$). Note that both the requirements for the minimum power and the optimum densities are very similar to those of ELMy H-mode. The main distinction between access to ELMy and EDA H-mode at Alcator C-Mod was a pedestal collisionality ν^* [3], which was typically higher in EDA H-mode ($\nu^* \geq 4$ [43]). In practice, ν^* was influenced by a particular plasma shape: $\kappa = 1.4$ – 1.5 , $\delta_u = 0.2$, $\delta_l = 0.8$ for ELMy H-mode and $\kappa = 1.6$ – 1.7 , $\delta_{u,l} = 0.3$ – 0.5 for EDA H-mode. Complementary factors were the L-mode density at the time of transition $n_{e,L}$, with EDA H-mode occurring more likely for $n_{e,L} > \frac{1}{4} n_{GW}$, and high $q_{95} > 3.5$ [44].

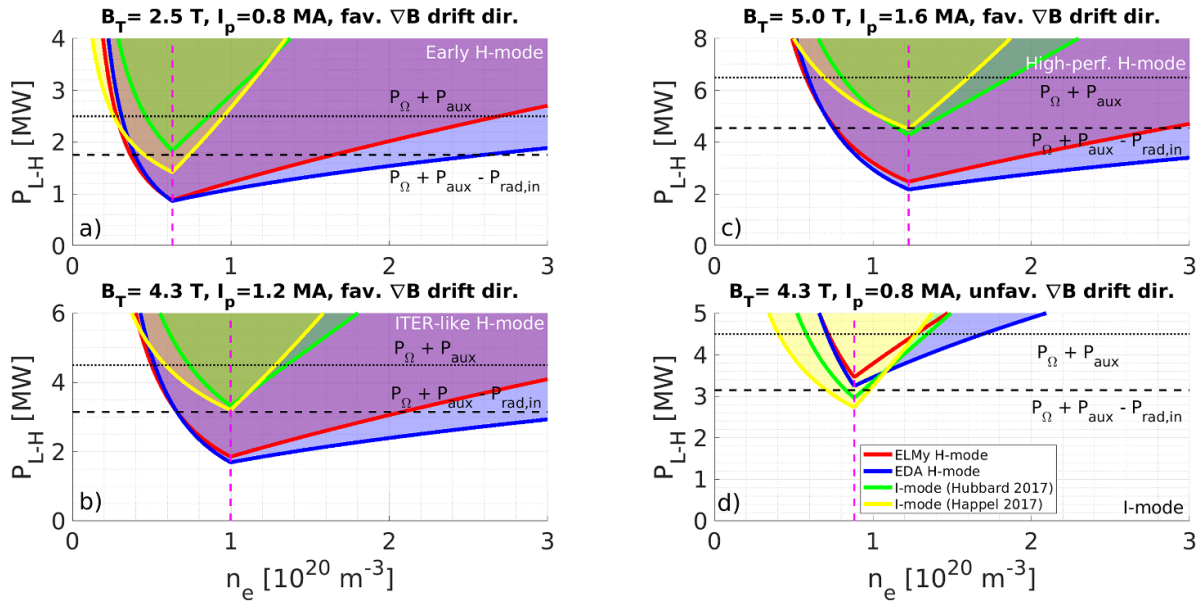


Figure 3. Power thresholds for accessing the ELMy H-mode, EDA H-mode and I-mode for the early H-mode scenario (a), ITER-like H-mode scenario (b), high-performance H-mode (c) and I-mode (d). Dotted horizontal lines indicate available heating power, and dashed lines indicate power crossing the separatrix, including 30% of the core radiated power.

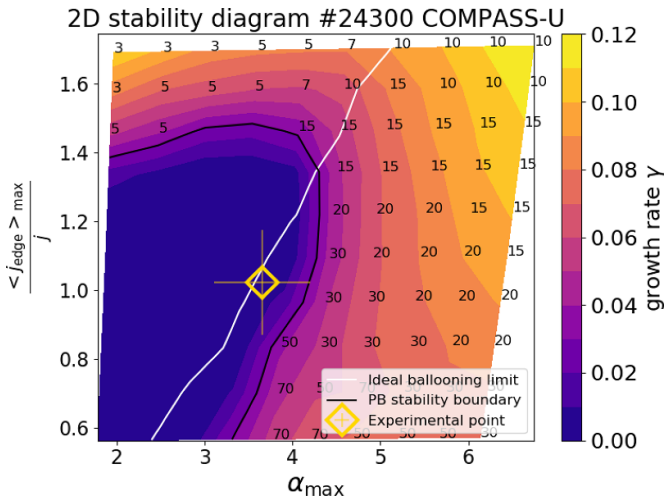


Figure 4. Pedestal stability calculations using the MISHKA code for the ITER-like H-mode.

Given the limited experience with EDA H-mode, it is currently not feasible to make reliable predictions, which would be able to make distinctions between ELMy and EDA H-mode. The default plasma shape of COMPASS Upgrade is closer to that used for EDA H-mode access at Alcator C-Mod, and the availability of ECRH appears to be relevant to the experimental recipe for EDA H-mode at both AUG and Alcator C-Mod. However, unlike Alcator C-Mod, COMPASS Upgrade will be equipped with a divertor cryopump and additional pumping capacities via the large NBI ducts, which may reduce ν^* and enable access to ELMy H-mode. The predicted pedestal profiles were analysed using the MISHKA code [45] to assess the pedestal stability, as shown in figure 4. For ITER-like H-mode, the pedestal is marginally unstable with

respect to the ballooning limit, which suggests an ELMy H-mode regime.

The sparseness of the available experimental data represents a formidable challenge for the design of future scenarios in COMPASS Upgrade but, at the same time, it justifies the need for a new machine, which will be able to fill the gaps defined by the parameter spaces of the currently operated and past machines.

4.3. I-mode

I-mode [33] is characterised by the presence of an edge transport barrier for energy but absence of such a barrier for particles, which allows a high core temperature to be reached but prevents accumulation of impurities. The lack of a density pedestal makes I-mode an ideal tool for investigation of scrape-off layer (SOL) conditions at low collisionality. The transport in the edge plasma is regulated by the weakly-coherent mode, which prevents the plasma from becoming peeling–ballooning unstable. Just like EDA H-mode, it is a perspective candidate for future machines due to the absence of ELMs, although some intermittent transport appears in the form of pressure relaxation events [46]. Currently, the studies of I-mode focus on its compatibility with detachment [47]. The power threshold P_{L-I} for I-mode access observed at Alcator C-Mod (where this mode was discovered) was reported by Hubbard *et al* [48] as:

$$P_{L-I, \text{Hubbard}} (\text{MW}) = 0.162 B_T^{0.26} [\text{T}] n_e [10^{20} \text{ m}^{-3}] S [\text{m}^2]. \quad (4)$$

Another scaling method was derived by Happel at AUG [49]. Assuming that the key quantity for accessing any of the high-confinement regimes is actually the power density (rather

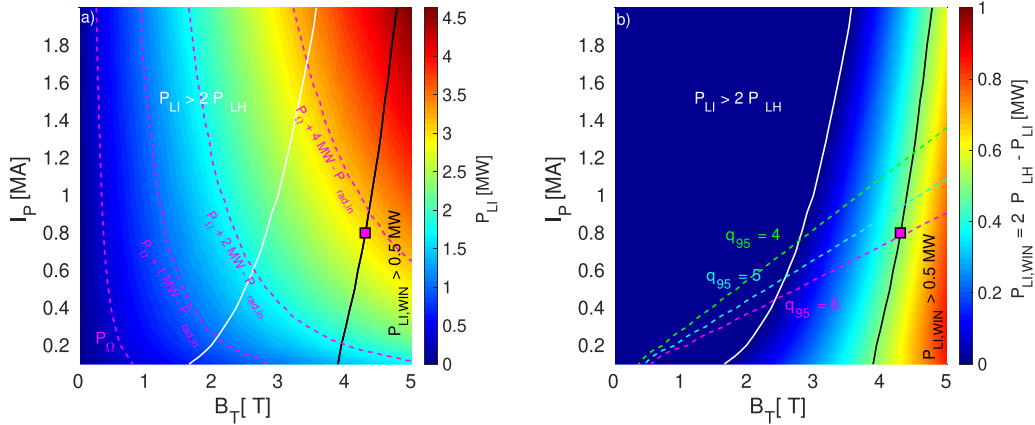


Figure 5. The operating window for I-mode in terms of the required power to achieve it in the unfavourable configuration at optimal density $n_{L-H,\min}$ (a), and as a difference between the power threshold for H-mode access and the power threshold for I-mode access $P_{LI,WIN}$ (b). The white line indicates $P_{LI,WIN} = 0$, and the black line indicates $P_{LI,WIN} = 0.5$ MW.

than the input power itself), this scaling can be extended to allow predictions for machines with different separatrix areas:

$$P_{L-I, \text{Happel}} \text{ (MW)} = 0.099 B_T^{0.39} [\text{T}] n_e^{1.36} [10^{20} \text{ m}^{-3}] S [\text{m}^2]. \quad (5)$$

As in ELMy H-mode, these scalings characterise only the high-density branch of the dependence. The scaling for optimum density for I-mode access has not been published but data from Alcator C-Mod suggest that it is similar to equation (1) and that similarly to ELMy H-mode, the power threshold rises sharply below this optimum [50].

There are several aspects of P_{L-I} worth attention. The dependence on B_T , which has a lower exponent than in P_{LH} (equation (1)), makes I-mode a perspective candidate for future high-field machines such as SPARC and ARC. However, in any of the scenarios envisaged for COMPASS Upgrade, $P_{L-I} \geq P_{L-H}$ when ∇B drift points towards the active X-point, which prevents stable I-mode operation. For this reason the I-mode scenario requires ∇B drift to be pointing away from the active X-point (as shown in figure 5), which effectively doubles P_{L-H} (note that equations (4) and (5) were developed using experimental data obtained in this configuration). In COMPASS Upgrade, the reversal of B_T will also require reversal of the I_p direction for the LSN plasmas because of the single toroidal bevel front shaping for the divertor PFCs. For USN plasmas, this will not be necessary since the top open divertor will accept both directions of plasma helicity. Since operating the NBI systems with reversed I_p should result in high first-orbit losses [51], the LSN I-mode scenario will make use of the steerable NBI unit and ECRH heating.

The operating space for I-mode in terms of plasma heating for different values of B_T and I_p is shown in figure 5. The window for I-mode access is defined as a difference between the threshold for H-mode (in an unfavourable configuration) and I-mode access:

$$P_{LI,WIN} = 2P_{L-H} - P_{L-I, \text{Hubbard}}. \quad (6)$$

$P_{LI,WIN}$ is calculated at optimal density, which coincides with $n_{L-H,\min}$. The best conditions for accessing I-mode are at high

B_T and low I_p . For $B_T < 4$ T, the operating window for I-mode is smaller than 0.5 MW, which is considered too small for practical exploitation, even with the use of dedicated real-time control systems. On the other hand, a plasma current below 0.8 MA at high B_T yields $q_{95} > 6$, which cannot be considered as ITER- or DEMO-relevant scenarios. These boundary conditions define an optimal I-mode scenario with $B_T \sim 4.3$ T, $I_p \sim 0.8$ MA and $n_e = 1 \times 10^{20} \text{ m}^{-3}$, requiring 4 MW of auxiliary heating power (as shown in figure 3(d)). This operating point should be available for both LSN (with 2 MW of ECRH and 2 MW of co-injection NBI power) and USN plasmas (with 6 MW of total heating power).

4.4. QH-mode

QH-mode [52] is another example of a stable ELM-free regime, where intermittent ELMy transport is replaced by continuous transport driven by an edge harmonic oscillation. QH-mode is particularly attractive, because it serves as an entry point to the *wide pedestal H-mode*, which features superior pedestal parameters and confinement properties [53]. The key access condition to QH-mode appears to be a sufficient amount of $E \times B$ rotational shear, which was traditionally achieved by counter-injection of NBI. However, recent experiments at DIII-D have proved that QH-mode can also be achieved with NBI co-injection [34]. The operation with NBI counter-injection in COMPASS Upgrade will be possible for both USN and LSN using the steerable NBI unit. Unlike the other modes described earlier, to our knowledge, there is not yet a formulated access condition for QH-mode in terms of the required injected power, and its compatibility with plasma detachment has also not been demonstrated yet; both of these topics will be studied at COMPASS Upgrade.

4.5. QCE mode

QCE mode (previously dubbed the *small ELM regime*) was developed at AUG in highly shaped plasmas with high separatrix density. In this mode the size of ELMs reduces and the

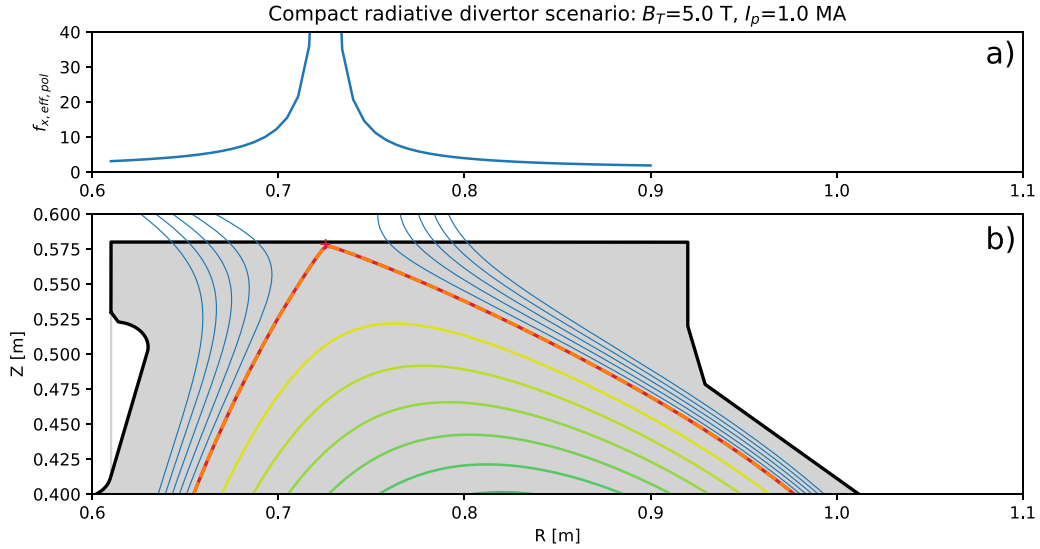


Figure 6. A scenario demonstrating the CRD plasma configuration at the upper initial open divertor with large effective poloidal flux expansion (a) and the strike point in close vicinity to the target plate (b).

intermittent ELM transport is replaced by a continuous flow of filaments to the divertor. While these filaments are significantly smaller than the filaments of large ELMs, they feature increased power decay length compared to the inter-ELM values [5]. Recently, QCE mode was also achieved at JET [54]. At the time of writing, no generalised conditions for access to QCE mode were formulated; however, the magnitude of high triangularity, which was required for QCE access at AUG, is actually on the lower boundary of the range of triangularities available for COMPASS Upgrade. The access to this regime will therefore probably be only limited by the achievable separatrix density (and related limitations of the auxiliary heating systems).

4.6. X-point radiating regime

XPR has recently been discovered at AUG [10]. Typically, it is accessed from ELMy H-mode by injection of impurities (such as Ar) in the divertor region. Once the X-point radiator (a concentrated ring of radiation in the vicinity of the X-point) forms, a real-time feedback system is used to keep it at optimal distance above the X-point. This regime appears to be very promising for future reactors as it combines relatively good confinement with high radiated power (up to 90%) in the edge plasma and the absence of ELMs. The design of the bolometry system at COMPASS Upgrade will be optimised to allow the required real-time control and subsequent investigation of its stability in the case of very narrow power decay lengths.

4.7. Compact radiative divertor

The CRD regime has recently been achieved at AUG [36] as a variant of the XPR. In this regime, the X-point is positioned close to the divertor plates, which leads to a large flux expansion in the vicinity of the strike points. This plasma configuration leads to reduced surface heat fluxes and, moreover,

facilitates detachment via impurity seeding. The regime is typically accompanied by small ELMs at high frequency; however, it retains the confinement quality of Type I ELMy H-mode. CRD scenarios will make use of the upper open divertor, where the X-point can be positioned in close proximity to the divertor target, leading to a large flux expansion, as shown in figure 6.

5. Predictions of pedestal properties

5.1. Pedestal density

Predictive modelling of pedestal density represents a remarkable blind spot in contemporary fusion research. While there are sophisticated tools to predict the pedestal pressure (such as EPED [55]), our literature review yielded only sparse cues on how to predict pedestal density. Design considerations for future machines such as ITER or SPARC [56] typically circumvent this problem by performing a scan of pedestal densities and selecting a scenario with the maximum pressure (which is needed to achieve the desired high Q). However, due to limitations of the heating systems, reliable predictions of natural H-mode plasma densities [57] are essential for the design of scenarios of COMPASS Upgrade.

Concerning ELMy H-mode, measurements at JET (with a carbon wall) and DIII-D yielded the following scaling by Schneider [58]:

$$n_{e,\text{ped|DIII-D,JET}} [\times 10^{19} \text{ m}^{-3}] = 2.4 I_p^{0.8} [\text{MA}] B_T^{0.5} [\text{T}]. \quad (7)$$

Experience with the tungsten wall at AUG suggested agreement with the parametric dependencies. However, the absolute pre-factor was twice as large, leading to the following estimate:

$$n_{e,\text{ped|Schneider}} [\times 10^{19} \text{ m}^{-3}] = 4.8 I_p^{0.8} [\text{MA}] B_T^{0.5} [\text{T}]. \quad (8)$$

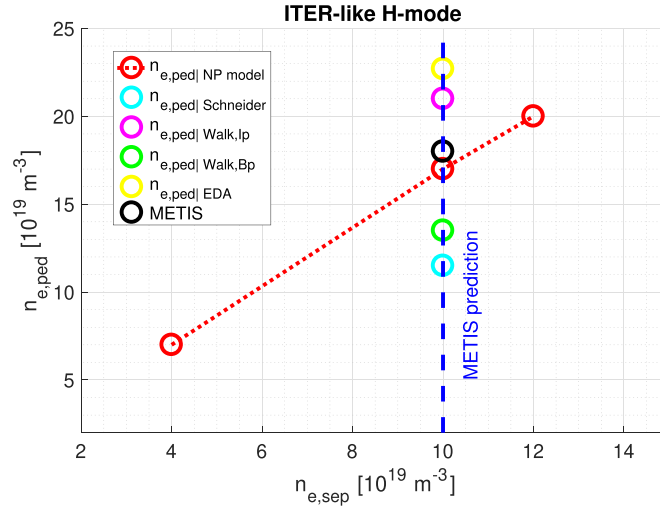


Figure 7. Predictions of the pedestal density as a function of the separatrix density by the neutral penetration model and the semi-empirical scaling models for the ITER-like H-mode scenario.

Table 3. Predictions of pedestal density in ELMy and EDA H-mode discharges compared to the ECRH cutoff density n_{cutoff} . All densities are given in $[10^{19} \text{ m}^{-3}]$.

| Scenario | $n_{e,\text{ped}} \text{Schneider}$ | $n_{e,\text{ped}} \text{Walk},I_p$ | $n_{e,\text{ped}} \text{Walk},B_p$ | $n_{e,\text{ped}} \text{EDA}$ | n_{cutoff} |
|---|-------------------------------------|------------------------------------|------------------------------------|-------------------------------|---------------------|
| Early H-mode | 6.3 | 11.5 | 9.0 | 17.6 | 12 |
| ITER-like H-mode | 11.5 | 21 | 13.5 | 22.7 | 21 |
| High perf. H-mode | 15 | 28 | 18 | 27 | 25 |
| $I_p = 2 \text{ MA}, B_T = 5 \text{ T}$ | 19 | 34 | 23 | 33 | 25 |

Measurements of the pedestal density in ELMy H-mode discharges at Alcator C-Mod were investigated by Walk [59]. Again, an approximately linear dependence on plasma current was identified and a re-calibration of equation (7) to match Alcator C-Mod data yields an even larger absolute pre-factor:

$$n_{e,\text{ped}}|\text{Walk},I_p [\times 10^{19} \text{ m}^{-3}] = 8.7I_p^{0.8} [\text{MA}] B_T^{0.5} [\text{T}]. \quad (9)$$

Walk has also investigated the dependence of pedestal density on the poloidal magnetic field B_p . With a great level of approximation, his results can be characterised as:

$$n_{e,\text{ped}}|\text{Walk},B_p [\times 10^{19} \text{ m}^{-3}] = 25 \pm 10B_p [\text{T}]. \quad (10)$$

Note that the last two scaling laws were derived on a single machine and, as such, may lack dependencies on parameters which are fixed for a given tokamak. However, given the close proximity of the design of COMPASS Upgrade and Alcator C-Mod, we neglect these dependencies in the first approximation.

In EDA H-mode, the scaling reported by Tolman *et al* [3] from Alcator C-Mod suggests:

$$n_{e,\text{ped}}|\text{EDA} [\times 10^{20} \text{ m}^{-3}] = 3.57I_p^{0.52} [\text{MA}] n_{e,L}^{0.52} \times [\times 10^{20} \text{ m}^{-3}] B_T^{-0.38} [\text{T}]. \quad (11)$$

Interestingly, in this regime the pedestal density depends on the density at L-H transition $n_{e,L}$. This allows for some optimisation; however, it is not expected that $n_{e,L}$ could be lower than the optimum density $n_{L-H,\text{min}}$ predicted by Ryter.

Recent initial simulations performed by a neutral penetration model [60] allowed one to make predictions of pedestal density as a function of the separatrix plasma $n_{e,\text{sep}}$ density and separatrix neutral density $n_{0,\text{sep}} \sim 1 \times 10^{16} \text{ m}^{-3}$ (deduced from dedicated KN1D simulations [28] and Alcator C-Mod measurements [61]). The results for ITER-like H-mode are summarised in figure 7. Using the separatrix density predicted by METIS ($n_{e,\text{sep}} = 10 \times 10^{19} \text{ m}^{-3}$ for the ITER-like H-mode scenario) the predicted pedestal density is located between the predictions of $n_{e,\text{ped}}|\text{Walk},I_p$ and $n_{e,\text{ped}}|\text{Walk},B_p$ models. The METIS calculations were adapted to match the prediction of the neutral penetration model.

The predictions of the pedestal density in ELMy and EDA H-modes are summarised in table 3. It can be seen that for early H-mode and ITER-like H-mode all the scalings for ELMy H-mode predict densities which are below the ECRH cutoff density n_{cutoff} (note that this density varies according to the heating scheme used for a given B_T). However, achieving EDA H-mode can already be challenging and may require reduction of the plasma current. For reference, the scenario #6400 with maximum engineering parameters of the machine is also presented. Here, efficient heating of H-mode discharges would be problematic, and this was the primary reason for the

development of scenarios with reduced plasma current as the baseline H-mode scenarios.

5.2. Pedestal pressure

Pedestal structure predictions from the EPED model [55] are shown as a function of pedestal density and global normalised beta. For the $\beta_N = 1.1$ case, both the simplified EPED1 model and the full EPED1.6 model (where both the kinetic ballooning mode and peeling–ballooning mode constraints are directly calculated for each case) predictions are shown in figure 8. At low density ($< 3 \times 10^{20} \text{ m}^{-3}$), the pedestal is predicted to be limited by current-driven peeling modes, and the predicted pressure increases with density. At high density, the pedestal is limited by pressure-driven ballooning modes, and the predicted pressure decreases with density. Optimal pedestal pressure is achieved at a density near the transition ($\sim 3 \times 10^{20} \text{ m}^{-3}$), and, near that density, pedestal pressures approaching the EPED predicted ITER baseline value ($p_{\text{ped}} \sim 100 \text{ kPa}$) and greater than the highest value achieved in any prior experiment are predicted. The current record was measured by Alcator C-Mod with $p_{\text{ped}} \sim 80 \text{ kPa}$ [62].

6. Plasma shapes

Recent studies have highlighted the role of triangularity on various plasma properties. High triangularity leads to stabilisation of the peeling–ballooning instability in the edge, producing regimes with small ELMs or with quasi-continuous transport [5]. High triangularity is also believed to increase the pedestal height [4]. As such, ITER will operate with $\delta \sim 0.5$, which is higher than what is routinely operated on contemporary machines in single-null plasmas. The ITER plasma shape served as a reference for the plasma shape of all main scenarios, which will be one of the unique features of COMPASS Upgrade. In addition, the positioning of PFCs will allow a wide range of triangularities, $0.35 < \delta < 0.65$ (as demonstrated in figure 9), enabling detailed studies of the importance of δ .

Apart from single-null plasmas, COMPASS Upgrade will also be capable of achieving alternative divertor configurations, such as double null or snowflake, as already reported in [17].

7. Power exhaust

7.1. Divertor heat fluxes

Following the pioneering study by Eich [7], a number of multi-machine scalings of H-mode power decay length have been developed [63, 64] using various quantities as scaling factors. For the purpose of our predictions, we have selected the Brunner scaling [63], because it was developed on a similar machine (Alcator C-Mod) and it also allows one to predict λ_q for L-mode and I-mode scenarios. Nevertheless, the predictions of λ_q for COMPASS Upgrade via different scaling

formulas were quite similar; for the scenarios considered in this work it was in the range of 0.6–1.2 mm.

Such small values of λ_q enable the ability to deliver extremely high surface heat fluxes onto the divertor targets in the range of $q_{\text{surf}} \sim 100 \text{ MW m}^{-2}$ in fully attached plasmas. These fluxes are relevant to off-normal conditions in next-step devices, for example, in case of accidental loss of detachment. Since the divertor tiles for COMPASS Upgrade are inertially cooled, the presence of such heat fluxes imposes a constraint on the duration of the discharge flat-top so that the surface temperature of the divertor tiles remains sufficiently low to prevent damage to the PFCs (here, considered as $T_{\text{surf}} < 2000 \text{ }^\circ\text{C}$). The surface heat flux can be predicted using an energy balance between the power crossing the separatrix and reaching the divertor plate:

$$q_{\text{peak,surf}} = f_t \frac{P_{\text{sep}} (1 - f_{\text{rad,SOL}})}{2\pi \lambda_{\text{int}} R_t f_{x,\text{pol}}}, \quad (12)$$

where f_t is the fraction of power reaching the particular divertor target (assuming 2:1 power sharing for the outer and inner target, respectively), P_{sep} is the power crossing the separatrix, $f_{\text{rad,SOL}}$ is the radiated fraction in the SOL, λ_{int} is the integral power decay length equal to $\lambda_q + 1.64 \times S$ [7] (here, assuming $S = \lambda_q/2$), R_t is the major radius of the target (equal to $\sim 0.625 \text{ m}$ and 0.810 m for the inner and outer vertical targets, respectively) and $f_{x,\text{pol}}$ is the poloidal flux expansion (typically equal to 6.5 for the bottom closed divertor).

The evolution of surface temperature due to impinging heat flux can be estimated using a simple 1D model of heat conduction [65]

$$T_{\text{surf}}(t) = T_{\text{surf},0} + q_{\text{peak,surf}} \frac{2}{\sqrt{\pi}} \sqrt{\frac{t}{c_v \kappa_s}}, \quad (13)$$

where c_v and κ_s are heat volumetric capacity and heat conduction, respectively (with approximate values of $2.49 \text{ MJ m}^{-1} \text{ K}^{-1}$ and $172 \text{ W m}^{-1} \text{ K}^{-1}$ for tungsten), and $T_{\text{surf},0}$ is the initial surface temperature (assumed to be equal to $20 \text{ }^\circ\text{C}$). This model can be easily inverted to provide a time delay $t_{\text{crit,1D}}$ needed to reach the critical temperature, $T_{\text{surf,crit}} = 2000 \text{ }^\circ\text{C}$. Table 4 shows the predictions for selected scenarios. The early L-mode and H-mode scenarios should not be significantly limited in duration by the heating of the PFCs; however, the high-performance H-mode scenario allows only a flat-top duration below 300 ms, which is not sufficient for physics studies. One solution is to introduce impurities such as nitrogen in the divertor region to enhance power dissipation. This process is capable of increasing $f_{\text{rad,SOL}}$ up to 90%—such values were achieved on Alcator C-Mod [66] and AUG tokamaks [10]. Table 4 shows the calculations for a more conservative value of $f_{\text{rad,SOL}} = 80\%$. In such a case all the scenarios allow for a flat-top duration longer than 1 second, which is the pulse limit of the NBI sources.

The simplified 1D model was cross-checked for selected cases against a more complex 3D model consisting of a combination of the PFCflux code [67] (predicting the heat flux distribution on divertor tiles) and a 3D ANSYS model for heat

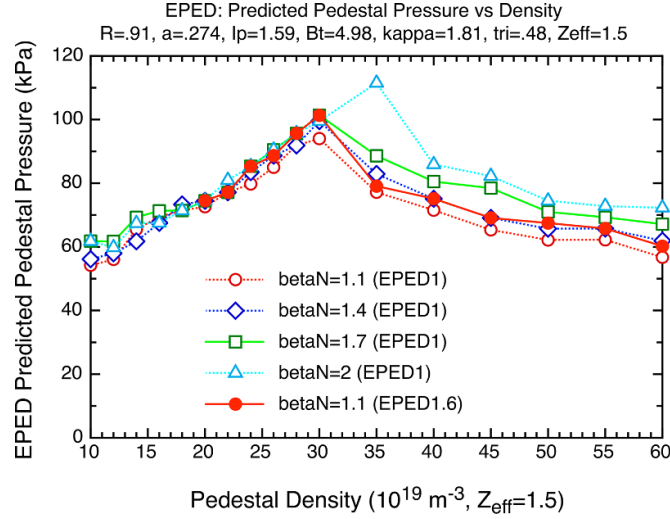


Figure 8. Predictions of pedestal pressure as a function of pedestal density for the high-performance H-mode calculated by EPED1 and EPED1.6.

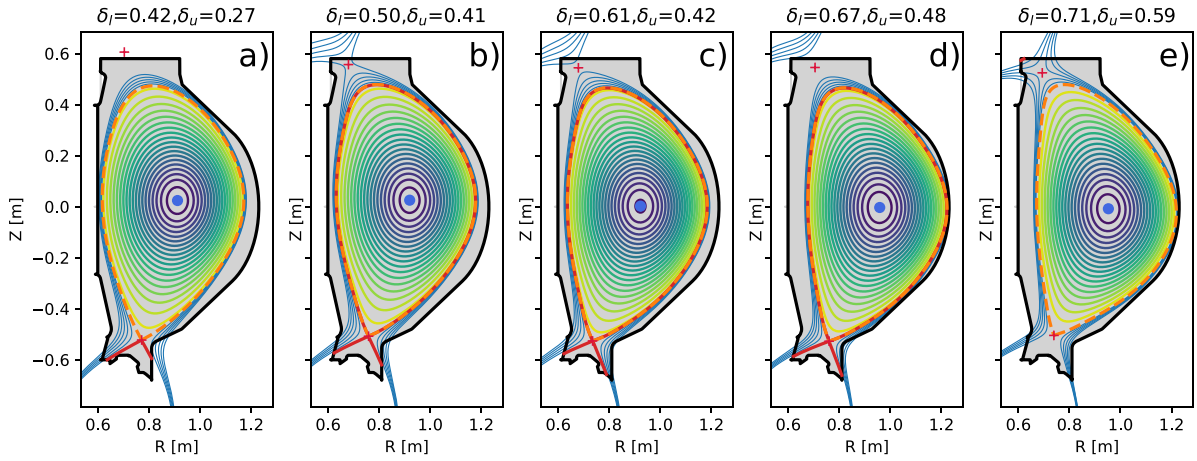


Figure 9. (a)–(e) Scenarios with plasma triangularities ranging from 0.35 to 0.65. Upper and lower triangularity values are mentioned in each panel title.

Table 4. Predictions of divertor surface heat fluxes and the critical time t_{crit} required to reach a surface temperature of 2000 °C (with initial temperature 300 K).

| | Early L-mode | Early H-mode | ITER-like H-mode | High perf. H-mode |
|--|--------------|--------------|------------------|-------------------|
| P_{sep} (MW) | 0.7 | 1.8 | 3.2 | 4.7 |
| λ_q (mm) | 1.98 | 1.37 | 1.0 | 0.81 |
| $q_{\text{surf},1\text{D}}(f_{\text{rad},\text{SOL}} = 0\%)$ (MW m^{-2}) | 3.1 | 17 | 37 | 76 |
| $q_{\text{surf},3\text{D}}(f_{\text{rad},\text{SOL}} = 0\%)$ (MW m^{-2}) | 8.4 | 32 | 74 | 148 |
| $q_{\text{surf},1\text{D}}(f_{\text{rad},\text{SOL}} = 80\%)$ (MW m^{-2}) | 0.61 | 3.4 | 7.4 | 15 |
| $t_{\text{crit},1\text{D}}(f_{\text{rad},\text{SOL}} = 0\%)$ (s) | >10 | 4.5 | 1.0 | 0.23 |
| $t_{\text{crit},3\text{D}}(f_{\text{rad},\text{SOL}} = 0\%)$ (s) | >10 | 5.9 | 0.54 | 0.08 |
| $t_{\text{crit},1\text{D}}(f_{\text{rad},\text{SOL}} = 80\%)$ (s) | >10 | >10 | >10 | 5.7 |

conduction in the tungsten tiles with temperature-dependent thermal properties. The prediction of peak heat fluxes and critical times are labelled as $q_{\text{surf},3\text{D}}$ and $t_{\text{crit},3\text{D}}$, respectively, in table 4. The 3D model takes into account the shaping of the W divertor tiles (0.5 mm toroidal bevel), leading to an increase in the peak surface heat flux by a factor of ~ 1.9 . An

additional increase by an approximate factor ~ 1.5 occurs due to temperature dependence of the material constants (in particular κ_s , which decreases with increasing temperature). It also models the heat diffusion in the bulk material (enabled by the relatively small poloidal extent of the heat flux footprint due to short λ_q), which can extend t_{crit} . However, this

beneficial mechanism is dependent on the ratio of heat diffusion time scale and the actual t_{crit} and, therefore, it scales unfavourably with the impacting heat flux. Altogether, these additional effects partially compensate each other and can be crudely approximated by the following semi-empirical relation:

$$t_{\text{crit},3\text{D}}/t_{\text{crit},1\text{D}} \approx 0.6\sqrt{t_{\text{crit},1\text{D}}} \approx 0.6\frac{\sqrt{\pi}}{2} \times (T_{\text{surf,crit}} - T_{\text{surf},0}) \frac{\sqrt{c_v k_s}}{q_{\text{peak,surf}}}. \quad (14)$$

7.2. Detachment

Detachment is a regime of SOL transport, which is characterised by extensive volumetric power dissipation. As such, it is the preferred regime for ITER and next-step devices, since it allows one to protect the divertor PFCs from excessive particle and heat fluxes. Despite its popularity, practical detection of detachment is the subject of a wide spectrum of approaches: for example, by measuring the reduction of target T_e [68], probe saturation current roll-over [69] or the movement of the CIII radiation front [11]. However, a reduction in divertor heat fluxes may not always be proof of detachment; a very similar effect can also be achieved by core radiation [70], which is expected to be essential, e.g. for DEMO. Compelling experimental proof of detachment can be obtained by detecting significant pressure gradients between upstream and downstream locations [71].

COMPASS Upgrade will have a prominent advantage for investigation of detachment and its effect on heat fluxes. As documented in section 7.1, the high-power scenarios are expected to generate extremely large heat fluxes in attached conditions. Therefore, substantial power dissipation will be required to prevent overheating of the divertor PFCs. Even if a large fraction of P_{sep} will be dissipated, the impacting surface heat fluxes will be on a par with ITER's material limit of 10 MW m^{-2} . This will allow to one investigate such heat and particle fluxes by the divertor diagnostics in contrast to many contemporary machines, where heat fluxes in detached plasmas typically yield poor signal to noise ratio measurements [69].

A detachment qualifier q_{det} [72, 73] is a simplified metric capable of predicting the transition into the detachment state:

$$q_{\text{det}} = 1.3 \frac{P_{\text{sep}}}{R} \frac{0.005}{\lambda_{\text{int}}} \left(\frac{1.65}{R} \right)^{0.1} \left(\left(1 + \sum_z f_z c_z \right) p_{0,\text{div}} \right)^{-1}, \quad (15)$$

where c_z is the impurity concentration, f_z is the radiation efficiency of the respective impurity and $p_{0,\text{div}}$ is the divertor neutral pressure. Detachment is predicted for $q_{\text{det}} < 1$. Assuming nitrogen seeding ($f_{\text{N}_2} = 18$) and $P_{\text{sep}} = 3.1 \text{ MW}$ (corresponding to ITER-like H-mode with 30% core radiated fraction), the detachment operating space is presented in figure 10. Should the divertor neutral pressure reach 6 Pa (which was a pressure relevant to detached plasmas in Alcator C-Mod), the required

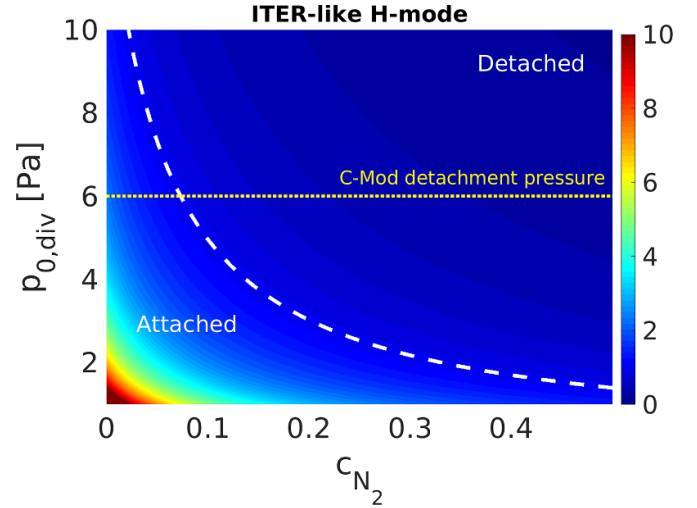


Figure 10. The detachment qualifier q_{det} as a function of the nitrogen concentration c_{N_2} and divertor neutral pressure $p_{0,\text{div}}$.

concentration of nitrogen in the divertor volume is about 7%. For early H-mode, detachment is predicted for divertor pressure above 5.6 Pa, even in the absence of any impurities. These initial results will, in future, be compared to detailed predictions of SOLPS-ITER modelling.

7.3. Liquid metals

One of the possible alternatives to solid PFCs is to employ metal sponges (i.e. capillary porous structures) wetted by an LM. Recent experiments in the two quasi-stationary plasma accelerator devices [74] have indicated that liquid Sn sustains the energy fluence $\epsilon_{\perp} = 3 \text{ MJ m}^{-2}$, which is beyond the expected peak ELM energy fluence of unmitigated Type I ELMs on ITER [75]. Remarkable power handling capabilities were demonstrated on the COMPASS tokamak for both liquid Li and liquid LiSn alloy at divertor surface heat loads $q_{\perp} = 12 \text{ MW m}^{-2}$ (relevant to ITER steady-state heat loading) and under more modest ELMs with a local peak energy fluence $\epsilon_{\perp} = 15 \text{ kJ m}^{-2}$ [76].

To interpret these experiments, a new simulation model dubbed *HeatLMD* [77] was developed, combining treatments of LM PFC, 3D heat conduction, sputtering, evaporation and vapour shielding of the incident plasma. HeatLMD was used to interpret recent LM experiments at AUG [78] and was also utilised to predict the behaviour of the LM divertor on the COMPASS Upgrade tokamak, including scenarios with extremely high-power density in the attached divertor $q_{\perp} \sim 100 \text{ MW m}^{-2}$ [79]. Further coupling with COREDIV [80] simulations predicted, for fully attached plasmas, that both the eroded Li and Sn might, however, cause unacceptably strong central plasma cooling and dilution within one second of plasma duration, even if the LM PFC was inertially cooled by a thick tungsten mass. Despite substantial differences in atomic mass between both metals, the effect on the plasma core cooling is expected to be very similar; the

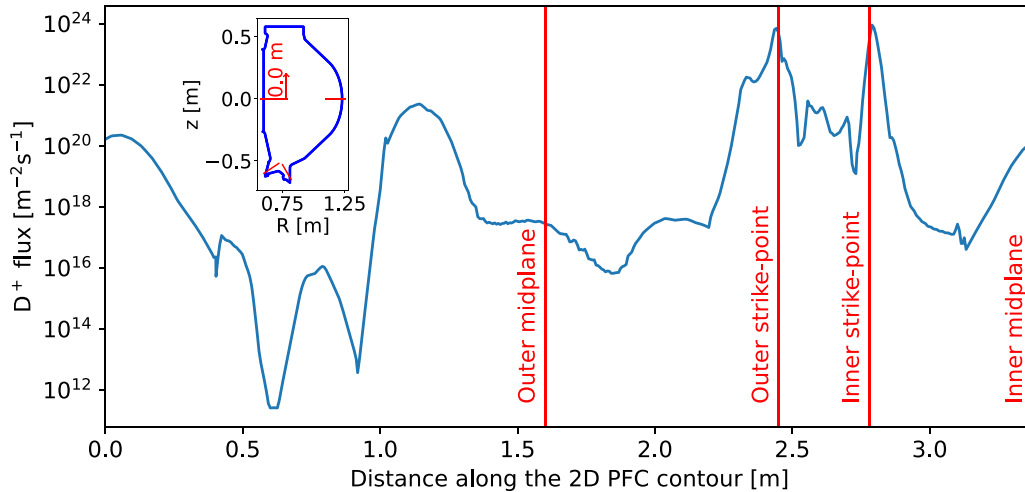


Figure 11. Surface particle flux to the first wall for the ITER-like H-mode scenario (without shoulder formation).

differences in cooling factors are compensated by different predicted LM concentrations in confined plasma. Future refining of this model, by including additional physics mechanisms using codes such as SOLPS-ITER, BIT1 and ERO 2.0, is planned to verify this prediction.

COMPASS Upgrade will be equipped with a divertor manipulator, mainly for material testing purposes [81], where different concepts of an LM divertor tile will be tested (different capillary porous materials and structure shapes, and different LMs). The pre-conceptual design of the LM divertor module is currently under development with the objective to contribute to the alternative DEMO divertor solution based on LM technology. Once an optimal solution for COMPASS Upgrade conditions is determined, a full toroidal ring of the LMD will be installed in the lower closed divertor.

8. Hot first wall operation

COMPASS Upgrade will have a unique capability to operate with elevated first wall temperature T_{wall} , up to 500 °C using in-vessel pipes with pressurised He or CO₂. This will allow one to explore conditions relevant to DEMO and future thermonuclear power plants, where high first wall temperature will help to optimise the power extraction [22, 23, 82].

An increased T_{wall} is known to significantly reduce the wall saturation time, meaning the time after which the wall is no longer capable of storing more impacting plasma particles. Recent investigation of this phenomena at the QUEST tokamak [83] suggests that at $T_{\text{wall}} = 500$ °C, and with the first wall flux exceeding $\Gamma_{\text{wall}} \sim 10^{21} \text{ m}^{-2} \text{ s}^{-1}$, the wall saturation time can be reached within less than 10 seconds and, therefore, possibly within the duration of the discharges of COMPASS Upgrade (assuming the wall saturation time scales as $\sim \sqrt{\Gamma_{\text{wall}}}$). The first wall fluxes for COMPASS Upgrade were estimated for the ITER-like H-mode scenario using simplified SOLPS-ITER simulations [84], where the fluxes were extrapolated to the first wall using the assumption of

$\lambda_n = 5 \text{ mm}$ (based on the relation $\lambda_n = \frac{21}{4} \lambda_q$ [85]), as shown in figure 11. Experimental observations from Alcator C-Mod suggest that such magnitudes of the particle flux are realistic [86].

This estimate suggests that some parts of the first wall, such as the upper stabilising plate or the divertor targets, are likely to reach wall saturation. Wall saturation may become even more likely in the case of shoulder formation [87], which can substantially increase the first wall fluxes. However, at the time of writing, no scaling law capable of predicting the density or particle flux profile in this regime exists. As such, it awaits to be investigated in detail at COMPASS Upgrade using, e.g. the midplane reciprocating manipulator.

The elevated T_{wall} will also aid experiments with LM components based on Li: at 500 °C the evaporation from the first wall components in combination with the presence of colder areas of the vessel (such as the NBI ducts) will prevent the formation of deposited layers, which may otherwise have detrimental effects on machine operation (e.g. by reducing the transparency of diagnostic optical elements). In addition, installation of a cold trap in the private flux regions is considered. The coating effect will not be present for Sn-based LM components; the evaporation rates of Sn are expected to be significantly lower than those of Li and, subsequently, the expected thickness of the deposited layers should not represent an operational issue. Moreover, the deposited Sn layer can be efficiently cleaned by a low-pressure Ar arc discharge [88].

Finally, the development and operation of tokamak and diagnostics systems [18] capable of withstanding such elevated temperatures represents a vital aspect of preparation for the operation of next-step devices.

9. Conclusions

COMPASS Upgrade will serve as a flexible tool to address the challenges associated with future thermonuclear reactors, thereby aiding their design and operation. Possessing a strong

magnetic field of 5 T, it can explore the properties of conventional ELM high-confinement mode as well as alternatives such as EDA H-mode, I-mode, QH-mode, QCE mode and the XPR. One of the objectives of the research at COMPASS Upgrade will be investigation of the compatibility of such alternative regimes with acceptable power exhaust solutions. The auxiliary heating scheme (ECRH and NBI heating) is fittingly compatible with the heating mix of ITER and DEMO.

One of the key areas of research will be the domain of the power exhaust, in particular the development of real-time control systems for detachment control and the development of LM technology, which is an alternative approach to conventional PFCs. These studies will be enabled by the ability to achieve a short power decay length ≤ 1 mm and extremely high divertor surface heat fluxes ~ 100 MW m⁻².







The device will be capable of achieving a wide range of positive triangularity, $0.35 < \delta < 0.65$, allowing one to investigate the role of plasma shape on confinement.

COMPASS Upgrade will also have a unique opportunity to operate with a hot first wall ($T_{\text{wall}} \leq 500$ °C), which will allow one to study plasma-wall interactions in reactor-relevant conditions and to test the compatibility of the tokamak subsystems and diagnostics with such conditions.

Acknowledgments

This work has been supported by MYES Projects #LM2018117 and GACR 22-03950S. M K would like to thank A E Hubbard and J W Hughes for insightful discussions on the properties of I-mode and EDA H-mode. The development of the liquid metal module is realised in collaboration with Eurofusion WP PRD-LM.

ORCID iDs

M. Komm  <https://orcid.org/0000-0001-8895-5802>
 F. Jaulmes  <https://orcid.org/0000-0002-8036-6517>
 M. Peterka  <https://orcid.org/0000-0003-4352-8895>
 J. Seidl  <https://orcid.org/0000-0002-8675-8431>
 P. Snyder  <https://orcid.org/0000-0002-0613-4232>
 J. Horacek  <https://orcid.org/0000-0002-4276-3124>
 D. Tskhakaya  <https://orcid.org/0000-0002-4229-0961>
 M. Hron  <https://orcid.org/0000-0003-3987-8040>

References

- [1] Kim S.H., Artaud J.F., Basiuk V., Dokuka V., Khayrutdinov R.R., Lister J.B. and Lukash V.E. 2009 *Plasma Phys. Control. Fusion* **51** 105007
- [2] Coda S. et al 2019 *Nucl. Fusion* **59** 112023
- [3] Tolman E., Hughes J., Wolfe S., Wukitch S., LaBombard B., Hubbard A.E., Marmar E., Snyder P. and Schmidtmayr M. 2018 *Nucl. Fusion* **58** 046004
- [4] Zhou C.X., Chan V., Chen J.L., Zhu Y.R., Jian X. and Zhuang G. 2023 *Phys. Plasmas* **30** 072508
- [5] Faitsch M. et al (The ASDEX Upgrade Team, The EUROfusion MST1 Team) 2021 *Nucl. Mater. Energy* **26** 100890
- [6] Zohm H. 2019 *J. Fusion Energy* **38** 3–10
- [7] Eich T. et al 2013 *Nucl. Fusion* **53** 093031
- [8] Chang C.S. et al 2017 *Nucl. Fusion* **57** 116023
- [9] Pitts R.A. et al 2019 *Nucl. Mater. Energy* **20** 100696
- [10] Bernert M. et al 2020 *Nucl. Fusion* **61** 024001
- [11] Ravensbergen T. et al 2021 *Nat. Commun.* **12** 1105
- [12] Brunner D. et al 2017 *Nucl. Fusion* **57** 086030
- [13] Khodunov I. et al 2021 *Plasma Phys. Control. Fusion* **63** 065012
- [14] Panek R. et al 2017 *Fusion Eng. Des.* **123** 11–16
- [15] Creely A., Brunner D., Mumgaard R., Reinke M., Segal M., Sorbom B. and Greenwald M. 2023 *Phys. Plasmas* **30** 090601
- [16] Ambrosino R. et al 2021 *Fusion Eng. Des.* **167** 112330
- [17] Vondracek P. et al 2021 *Fusion Eng. Des.* **169** 112490
- [18] Weinzettl V. et al 2023 *Fusion Eng. Des.* **191** 113545
- [19] Marmar E. et al 2015 *Nucl. Fusion* **55** 104020
- [20] Hanada K. et al 2017 *Nucl. Fusion* **57** 126061
- [21] Marmar E., Overskei D., Helava H., Chen K., Terry J. and Moos H. 1979 *Nucl. Fusion* **19** 485
- [22] Garofalo A.M. et al 2014 *Fusion Eng. Des.* **89** 876–81
- [23] Pamela J., Bécoulet A., Borba D., Boutard J.L., Horton L. and Maisonnier D. 2009 *Fusion Eng. Des.* **84** 194–204
- [24] Roth J. et al 2009 *J. Nucl. Mater.* **390** 1–9
- [25] Hirai T. et al 2016 *Nucl. Mater. Energy* **9** 616–22
- [26] Herrmann A. et al (ASDEX Upgrade Team) 2011 *Phys. Scr.* **2011** 014068
- [27] Jaulmes F. et al 2022 *Plasma Phys. Control. Fusion* **64** 125001
- [28] Jaulmes F., Zadvitskiy G., Bogar K., Imrisek M., Hromadka J., Cats S., Varju J., Komm M. and Panek R. 2021 *Nucl. Fusion* **61** 046012
- [29] Jaulmes F., Komm M., Grover O., Seidl J., Snyder P., Shyshkin O., Imrisek M., Zadvitskiy G., Gerardin J., Borodkina I. et al 2022 Scenarios for physics experiments in the compass upgrade tokamak *48th EPS Conf. on Plasma Physics (Maastricht, Netherlands)* (available at: <https://info.fusion.ciemat.es/OCS/EPS2022PAP/pdf/P2b.101.pdf>) (European Physical Society)
- [30] Cunningham G. 2013 *Fusion Eng. Des.* **88** 3238–47
- [31] Viezzer E. 2018 *Nucl. Fusion* **58** 115002
- [32] Hughes J. et al 2007 *Fusion Sci. Technol.* **51** 317–41
- [33] Whyte D. et al 2010 *Nucl. Fusion* **50** 105005
- [34] Burrell K., Osborne T., Snyder P., West W., Fenstermacher M., Groebner R., Gohil P., Leonard A. and Solomon W. 2009 *Phys. Rev. Lett.* **102** 155003
- [35] Faitsch M. et al 2023 *Nucl. Fusion* **63** 076013
- [36] Lunt T. et al 2023 *Phys. Rev. Lett.* **130** 145102
- [37] Coda S. et al (The TCV Team) 2021 *Plasma Phys. Control. Fusion* **64** 014004
- [38] Martin Y. et al 2008 *J. Phys.: Conf. Ser.* **123** 012033
- [39] Fundamenski W., Militello F., Moulton D. and McDonald D. 2012 *Nucl. Fusion* **52** 062003
- [40] Ryter F., Orte L.B., Kurzan B., McDermott R., Tardini G., Viezzer E., Bernert M. and Fischer R. (The ASDEX Upgrade Team) 2014 *Nucl. Fusion* **54** 083003
- [41] Greenwald M. et al 1997 *Nucl. Fusion* **37** 793
- [42] Gil L. et al 2020 *Nucl. Fusion* **60** 054003
- [43] Hughes J., Mossessian D., Hubbard A.E., LaBombard B. and Marmar E. 2002 *Phys. Plasmas* **9** 3019–30
- [44] Mossessian D. et al 2002 *Phys. Plasmas* **10** 1720
- [45] Mikhailovskii A., Huysmans G.T., Kerner W.O. and Sharapov S. 1997 *Plasma Phys. Rep.* **23** 844–57
- [46] Silvagni D. et al 2020 *Nucl. Fusion* **60** 126028
- [47] Happel T. et al 2021 *Nucl. Fusion* **61** 036026
- [48] Hubbard A.E. et al 2017 *Nucl. Fusion* **57** 126039
- [49] Happel T. et al 2016 *Plasma Phys. Control. Fusion* **59** 014004
- [50] Hubbard A.E. 2023 private communication
- [51] Jaulmes F., Ficker O., Weinzettl V., Komm M., Grover O., Seidl J., Zadvitskiy G., Macusova E. and Panek R. 2022 *J. Fusion Energy* **41** 16

- [52] Burrell K. *et al* 2001 *Phys. Plasmas* **8** 2153–62
- [53] Burrell K.H. *et al* 2016 *Phys. Plasmas* **23** 056103
- [54] Faitsch M. *et al* 2024 The quasi-continuous exhaust regime in ASDEX upgrade and JET 26th PSI Conf.
- [55] Snyder P., Groebner R., Hughes J., Osborne T., Beurskens M., Leonard A., Wilson H. and Xu X. 2011 *Nucl. Fusion* **51** 103016
- [56] Hughes J., Howard N., Rodriguez-Fernandez P., Creely A., Kuang A., Snyder P., Wilks T., Sweeney R. and Greenwald M. 2020 *J. Plasma Phys.* **86** 865860504
- [57] Borrass K. (ASDEX Upgrade Team and EFDA-JET Workprogramme collaborators) 2002 *Nucl. Fusion* **42** 1251
- [58] Schneider P.A. 2012 Characterization and scaling of the tokamak edge transport barrier Doctoral Ludwig–Maximilians–Universität München (available at: https://inis.iaea.org/search/search.aspx?orig_q=RN:45012779)
- [59] Walk J.J.R. 2014 Pedestal structure and stability in high-performance plasmas on Alcator C-Mod *PhD Thesis* Massachusetts Institute of Technology
- [60] Saarelma S., Connor J., Bilkova P. and Bohm P. 2023 *Nucl. Fusion* accepted (<https://doi.org/10.1088/1741-4326/ad4b3e>)
- [61] Reksoatmodjo R., Mordijck S., Hughes J., Lore J.D. and Bonnin X. 2021 *Nucl. Mater. Energy* **27** 100971
- [62] Hughes J. *et al* 2018 *Nucl. Fusion* **58** 112003
- [63] Brunner D., LaBombard B., Kuang A. and Terry J. 2018 *Nucl. Fusion* **58** 094002
- [64] Silvagni D. *et al* (The ASDEX Upgrade Team) 2020 *Plasma Phys. Control. Fusion* **62** 045015
- [65] Herrmann A. 2007 *Phys. Scr.* **2007** 234
- [66] Loarte A. *et al* 2011 *Phys. Plasmas* **18** 056105
- [67] Gerardin J., Balner V., Dejarnac R., Imrisek M., Jaulmes F., Komm M., Peterka M. and Vondracek P. 2023 *Fusion Eng. Des.* **194** 113731
- [68] Samuell C., Mclean A., Johnson C., Glass F. and Jaervinen A. 2021 *Rev. Sci. Instrum.* **92** 043520
- [69] Février O. *et al* 2020 *Plasma Phys. Control. Fusion* **62** 035017
- [70] Komm M. *et al* 2021 *Nucl. Fusion* **61** 036016
- [71] Komm M. *et al* 2019 *Nucl. Fusion* **59** 106035
- [72] Kallenbach A. *et al* 2015 *Nucl. Fusion* **55** 053026
- [73] Henderson S. *et al* 2023 *Nucl. Fusion* **63** 086024
- [74] Garkusha I. 2021 *Nucl. Fusion* **61** 116040
- [75] Eich T. *et al* 2017 *Nucl. Mater. Energy* **12** 84–90
- [76] Dejarnac R. *et al* 2020 *Nucl. Mater. Energy* **25** 100801
- [77] Horacek J. 2020 *Nucl. Mater. Energy* **25** 100860
- [78] Ceardle J. *et al* 2023 *Fusion Eng. Des.* **194** 113886
- [79] Horacek J. 2021 *Phys. Scr.* **96** 124013
- [80] Stankiewicz R. and Zagorski R. 2005 *J. Nucl. Mater.* **337** 191–5
- [81] Lukes S., Horacek J., Veselovsky V., Vondracek P., Sestak D., Adamek J., Weinzettl V. and Duran I. 2022 *J. Instrum.* **17** C02007
- [82] Abdou M., Morley N.B., Smolentsev S., Ying A., Malang S., Rowcliffe A. and Ulrickson M. 2015 *Fusion Eng. Des.* **100** 2–43
- [83] Hanada K., Hasegawa M., Onchi T. and Yoshida N. 2023 Recovery from wall saturation using temperature control of plasma facing wall on QUEST *Proc. 29th IAEA FEC Conf.*
- [84] Borodkina I. *et al* 2023 SOLPS-ITER simulations of high power scenarios in COMPASS upgrade tokamak 49th EPS Conf. on Plasma Physics (European Physical Society)
- [85] Eich T. *et al* 2018 *Nucl. Fusion* **58** 034001
- [86] LaBombard B., Umansky M., Boivin R., Goetz J., Hughes J., Lipschultz B., Mossessian D., Pitcher C. and Terry J. (Alcator Group) 2000 *Nucl. Fusion* **40** 2041
- [87] Carralero D. *et al* 2017 *Nucl. Fusion* **57** 056044
- [88] Mishra H., Mašek T., Turek Z., Čada M., Hubička Z., Kudrna P. and Tichy M. 2023 *J. Fusion Energy* **42** 36